

PAPER

# Ultrafast Carrier Dynamics in $\text{Ba}_6\text{Cr}_2\text{S}_{10}$ Modified by Toroidal Magnetic Phase Transition

To cite this article: Litong Jiang *et al* 2024 *Chinese Phys. Lett.* **41** 047802

View the [article online](#) for updates and enhancements.

## You may also like

- [Review—Temperature Dependence of Luminescence Intensity and Decay Time in  \$\text{Cr}^{3+}\$ -Activated Oxide and Fluoride Phosphors](#)  
Sadao Adachi
- [Intracavity  \$\text{Cr}^{3+}\$ :LiCAF + PPSLT optical parametric oscillator with self-injection-locked pump wave](#)  
H Maestre, A J Torregrosa and J Capmany
- [Review—Photoluminescence Properties of  \$\text{Cr}^{3+}\$ -Activated Oxide Phosphors](#)  
Sadao Adachi

## Ultrafast Carrier Dynamics in $\text{Ba}_6\text{Cr}_2\text{S}_{10}$ Modified by Toroidal Magnetic Phase Transition

Litong Jiang(姜丽桐)<sup>1</sup>, C. Y. Jiang(姜聪颖)<sup>1,3</sup>, Y. C. Tian(田义超)<sup>1,2</sup>, H. Zhao(赵惠)<sup>1,2</sup>, J. Zhang(张俊)<sup>1</sup>, Z. Y. Tian(田珍耘)<sup>1,4</sup>, S. H. Fu(付少华)<sup>1</sup>, E. J. Liang(梁二军)<sup>4</sup>, X. C. Wang(望贤成)<sup>1,2</sup>, Changqing Jin(靳常青)<sup>1,2,5</sup>, and Jimin Zhao(赵继民)<sup>1,2,5\*</sup>

<sup>1</sup>Beijing National Laboratory for Condensed Matter Physics, Institute of Physics, Chinese Academy of Sciences, Beijing 100190, China

<sup>2</sup>School of Physical Sciences, University of Chinese Academy of Sciences, Beijing 100049, China

<sup>3</sup>Strong-Field and Ultrafast Photonics Lab, Institute of Laser Engineering, Beijing University of Technology, Beijing 100124, China

<sup>4</sup>School of Physics & Laboratory of Zhongyuan Light, Zhengzhou University, Zhengzhou 450052, China

<sup>5</sup>Songshan Lake Materials Laboratory, Dongguan 523808, China

(Received 5 January 2024; accepted manuscript online 18 March 2024)

$\text{Ba}_6\text{Cr}_2\text{S}_{10}$  is a recently discovered magnetic material, in which the spins are aligned ferromagnetically in the  $ab$ -plane and anti-parallelly in a paired form along the  $c$ -axis. It is characterized as a quasi-one dimensional (1D) dimerized structure with a ferrotoroidic order, forming the simplest candidate toroidal magnetic (TM) order and exhibiting an anti-ferromagnetic-like transition at around 10 K. Time-resolved ultrafast dynamics investigation of the novel A–Cr–S (A: metal elements) family of quantum materials has rarely been reported. Here, we investigate the time-resolved pump-probe ultrafast dynamics of a  $\text{Ba}_6\text{Cr}_2\text{S}_{10}$  single crystal. A prominent change in the photo-excited carrier dynamics is observed at  $T_c = 10$  K, corresponding to the reported TM-paramagnetic phase transition. A potential unknown magnetic transition is also found at  $T^* = 29$  K. Our results provide new evidence for the TM magnetic transition in  $\text{Ba}_6\text{Cr}_2\text{S}_{10}$ , and shed light on phase transitions in TM quantum materials.

DOI: 10.1088/0256-307X/41/4/047802

There has been an enduring interest in the ternary chromium sulfides serial family (A–Cr–S, A: metal elements), due to its peculiar structural integration, which are composed of one-dimensional (1D) chains, two-dimensional (2D) layers, and three-dimensional (3D) frameworks.<sup>[1]</sup> This A–Cr–S family provides a particularly fruitful area for the exploration of novel quasi-1D dimerized structure materials with ferrotoroidic order.<sup>[2]</sup> Ferrotoroidic order is a primary ferroic order form, which is often regarded as the fourth magnetic order. The toroidal moment, which is generated by a head-to-tail magnetic moment, denotes the main parameter of this ferrotoroidic order. However, to date only a handful of ferrotoroidic materials have been reported, such as  $\text{LiCoPO}_4$ ,  $\text{LiFeSi}_2\text{O}_6$ , and  $\text{Co}_4\text{Nb}_2\text{O}_9$ ,<sup>[2]</sup> mainly due to their complex growth procedure under high pressure. Particularly, magnetic vortex patterns are hallmarks of such ferroic states, exhibiting a unique hysteretic poling of the ferrotoroidic domains.<sup>[3]</sup>

Recently we proposed this novel quasi-1D material  $\text{Ba}_6\text{Cr}_2\text{S}_{10}$ .<sup>[2]</sup> To date, four ternary barium chromium sulfides have been synthesized by Fukuoka *et al.*,<sup>[1,3]</sup> such as  $\text{Ba}_3\text{CrS}_5$ ,  $\text{Ba}_3\text{Cr}_2\text{S}_6$ ,  $\text{BaCr}_4\text{S}_7$ , and  $\text{Ba}_2\text{Cr}_5\text{S}_{10}$ , of which  $\text{Ba}_3\text{CrS}_5$  has a column structure with 1D chains of  $[\text{CrS}_6]_\infty$ , composed of face-sharing  $[\text{CrS}_6]$  octahedra surrounded by  $\text{Ba}^{2+}$  ions, similar to the  $\text{Ba}_6\text{Cr}_2\text{S}_{10}$  we investigate here.  $\text{Ba}_6\text{Cr}_2\text{S}_{10}$  is characterized as a quasi-1D

dimerized structure magnetic material with ferrotoroidic order, which is considered as the simplest toroidal magnetic (TM) order. At higher temperatures it becomes antiferromagnetic (AFM)-like, with a characteristic temperature at around 10 K.<sup>[2]</sup> As a new ferrotoroidic candidate material with a special magnetic order, the optical properties of  $\text{Ba}_6\text{Cr}_2\text{S}_{10}$  have not been widely investigated to date.

Time-resolved ultrafast pump-probe spectroscopy has been widely used to detect the photo-carrier properties in solids under extreme conditions, such as high pressure,<sup>[4,5]</sup> low temperature,<sup>[6,7]</sup> and strong magnetic field.<sup>[8,9]</sup> Due to its powerful ability to detect both single and collective quasiparticles, time-resolved pump-probe spectroscopy has been frequently used to investigate the high temperature cuprate superconductors,<sup>[7,10–14]</sup> iron-based superconductors,<sup>[6,15,16]</sup> topological materials,<sup>[17–21]</sup> and antiferromagnetic insulators,<sup>[22,23]</sup> etc. With this technique, various physical properties<sup>[7,24–28]</sup> of correlated materials have been investigated. Such an experimental means has rarely been employed to investigate the magnetic quantum materials of the A–Cr–S family.

In this work, we employ time-resolved ultrafast pump-probe spectroscopy to probe the photo-carriers in  $\text{Ba}_6\text{Cr}_2\text{S}_{10}$  to provide a dynamical characterization for the magnetic transition. Through temperature-dependent ex-

\*Corresponding author. Email: jmzhao@iphy.ac.cn

© 2024 Chinese Physical Society and IOP Publishing Ltd

periments, we have observed prominent changes in the ultrafast relaxation process at 10 K, which is consistent with the reported magnetic phase transition. In addition, another transition-like behavior is also observed at 29 K.

Our ultrafast pump-probe spectroscopy experiment configuration is similar to that in Refs. [6,29]. The femtosecond laser has 800 nm central wavelength, 80 fs pulse duration, and 250 kHz repetition rate. We separate the laser pulses into pump and probe beams and measure the differential reflectivity  $\Delta R/R_0$  of the reflected probe beam as a function of its delay time. The pump beam is modulated at 2 kHz by an optical chopper. The reflected probe beam is collected by a balanced photodetector to enhance the signal-to-noise ratio. In our temperature-dependent experiment, the diameters of pump and probe beams are 42 and 33  $\mu\text{m}$ , respectively. Because the sample is small ( $5 \mu\text{m} \times 15 \mu\text{m}$ ), a  $20\times$  objective is used to focus the beams on the sample (the diameters of focal spots for pump and probe beams are 7.89 and 6.20  $\mu\text{m}$ , respectively). The pump and probe fluences are maintained at 0.68 and 0.45  $\mu\text{J}/\text{cm}^2$ , respectively. Such fluences clearly correspond to a typical weak excitation regime.<sup>[6,15,30–32]</sup> The magnetic  $\text{Ba}_6\text{Cr}_2\text{S}_{10}$  single crystal is grown under high-pressure and high-temperature conditions, from which the needle-like single crystals with the width of approximately 100  $\mu\text{m}$  is selected.

We investigate the time-resolved relative differential reflectivity  $\Delta R/R_0$  for various temperatures. A typical data of this series at 22 K are presented in Fig. 1, where the magenta curve is based on the quantitative fitting function Eq. (1) discussed below. The right panel inset of Fig. 1 exhibits a schematic lattice structure for the toroidal AFM-like  $\text{Ba}_6\text{Cr}_2\text{S}_{10}$ , where the spin interval is  $a + b$  between the periodic magnetic units. Here,  $a$  and  $b$  are adjacent intervals along the  $z$ -axis, due to which the microstructure is different from that of a conventional AFM configuration (i.e.,  $a = b$ ). Being a long-range magnetic ordering, how this unique structure will lead to magnetic phase transition is intriguing. To clearly identify the relaxation components for the ultrafast process, we present the result in a logarithm scale in the left panel inset of Fig. 1. Three decay components can be clearly identified, corresponding to the fast (pink line), slow (blue line), and slower (purple line) components. Note that absolute values are considered. Thus, we employ a three-component exponential decay function to quantitatively analyze the photo-carrier dynamics:

$$\Delta R/R_0 = A_{\text{fast}} \exp(-t/\tau_{\text{fast}}) + A_{\text{slow}} \exp(-t/\tau_{\text{slow}}) + A_{\text{slower}} \exp(-t/\tau_{\text{slower}}) + A_0, \quad (1)$$

where  $A_{\text{fast}}$ ,  $A_{\text{slow}}$ , and  $A_{\text{slower}}$  denote amplitudes,  $\tau_{\text{fast}}$ ,  $\tau_{\text{slow}}$ , and  $\tau_{\text{slower}}$  represent lifetimes, and  $A_0$  is a component with very long lifetime that can be treated as a constant term. The  $A_0$  term may come from the indirect electron-hole recombination<sup>[33]</sup> or from much slower processes involving acoustic phonon-acoustic phonon scattering.<sup>[33]</sup> The data analysis based on Eq. (1) (solid curve) is shown in Fig. 1, which fits our experimental data well.

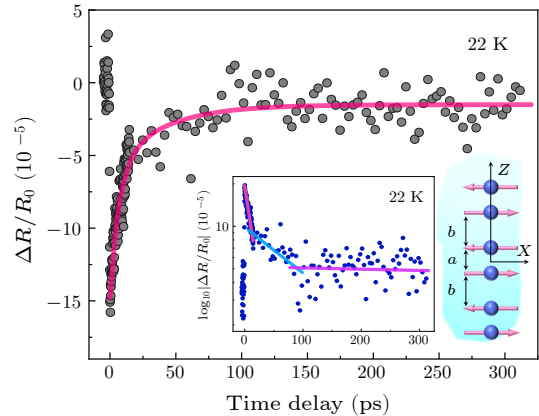


**Fig. 1.** Ultrafast relaxation of photo-excited carriers in  $\text{Ba}_6\text{Cr}_2\text{S}_{10}$  at 22 K. Solid magenta curve: fitting result based on Eq. (1). Right panel inset: schematic illustration of the unique spin alignment in TM  $\text{Ba}_6\text{Cr}_2\text{S}_{10}$ . Left panel inset: logarithm-scale presentation of the scanning trace to reveal three relaxation channels, corresponding to the fast (pink), slow (blue), and slower (purple) decay components. Note that absolute value of the  $\Delta R/R_0$  signal is analyzed.

The temperature dependence of the ultrafast relaxation dynamics is shown in Fig. 2. Figure 2(a) depicts the photo-induced differential reflectivity  $\Delta R/R_0$  within the time scale from  $-2$  to 15 ps (data are offset for clarity). With increasing temperature, the relaxation process exhibits a prominent weakening, with apparent flattening of the signal when temperature gradually approaches 60 K. During this process, both the amplitudes and lifetimes of the signals vary, marked by different colors. Again, the fitting results (solid curves) compare with our experimental data well [Fig. 2(a)]. Note that in the raw data of  $\Delta R$ , we did not observe a very prominent background before the arrival of the pump pulses, indicating that there is not much scattered pump stray light and there is no laser heating. In Fig. 2(b), we present the normalized  $\Delta R/R_0$  with increasing temperature (data are offset for clarity), particularly by presenting the data with a much longer scanning temporal range from  $-2$  to 320 ps. The data are normalized to the data at 5.7 K, which has the maximum absolute value at  $t = 0$  s. In Fig. 2(b), the slower component looks clearer.

In Fig. 2(c), we plot a 2D mapping of the  $\Delta R/R_0$  data given in Fig. 2(a). From Fig. 2(c), a color change at 10 K can be seen, which qualitatively marks a likely phase transition that is in line with the candidate TM ordering phase transition. At 29 K, another color change in a vertical stripe is identified, which may indicate another potential phase transition. In Fig. 2(d), we present a non-offset view of the data, which can be used to distinctly observe the trends in lifetime and amplitude variation.

We analyze the ultrafast relaxation process experimental data by employing Eq. (1). For various temperatures from 5.7 K to 60 K, the fitting results (red solid curves) are obtained (Fig. 3). For all the different temperatures, Eq. (1) fits the experimental data very well (solid curves). The curves exhibit different trends at different temperatures. We have carried out careful data analysis, which allows us to identify that the slow and slower components are

two separate components (Fig. S2 in the Supplementary Materials). Note that we developed a two-step scanning technique in our experiment. The only difference is the scanning step size. No other items were modified throughout the whole experiment. Thus, all the noise level before and after 18 ps is identical. Taking the data for 12 K for

an instance, in Fig. 2(d) the noise level is  $1 \times 10^{-4}$  for the data within 12 ps; in Fig. 3 the noise level is also  $1 \times 10^{-4}$  for the data within 18–300 ps. Furthermore, a replot better illustrates the identical detection noise level (Fig. S3 in the Supplementary Materials).

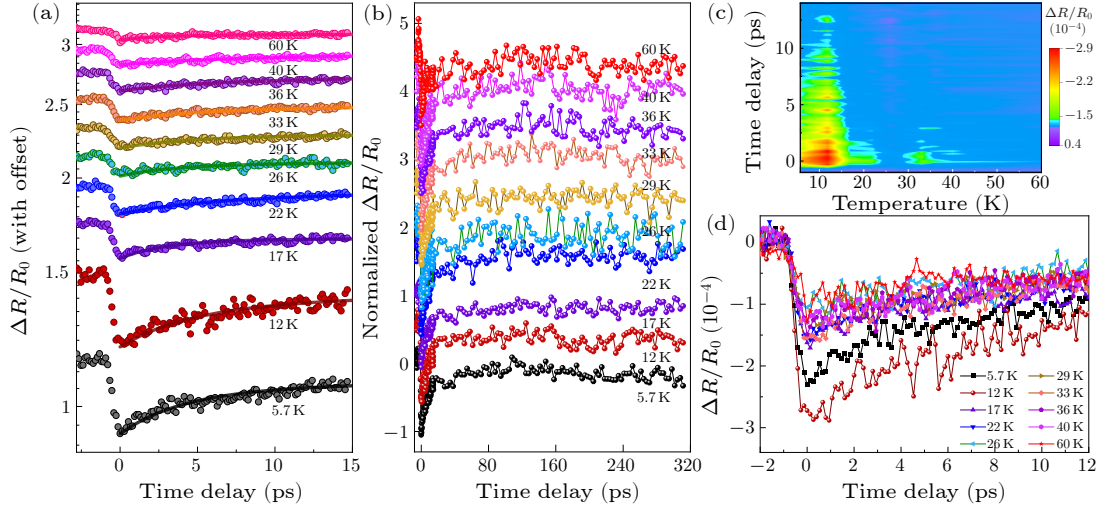


**Fig. 2.** (a) Temperature dependence of the photo-induced relative differential reflectivity  $\Delta R/R_0$  versus the delay time in the  $-2$ – $15$  ps temporal range (offset for clarity). (b) Normalized  $\Delta R/R_0$  signal in the  $-2$ – $320$  ps temporal range (offset). (c) Two-dimensional color map of ultrafast photo-carrier dynamics data as a function of both time delay and temperature. (d) Non-offset data to better reveal the variations in the ultrafast relaxation processes.

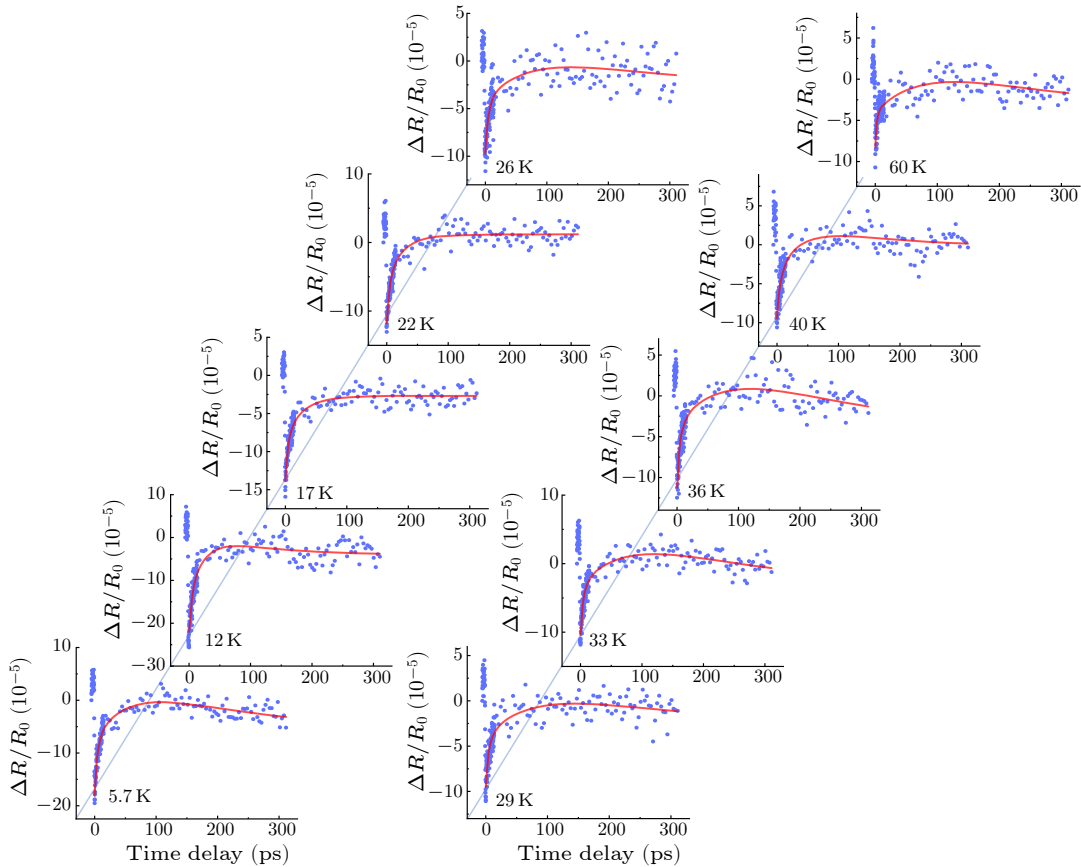


**Fig. 3.** Quantitative data analysis of the  $\Delta R/R_0$  signal in the temperature dependence experiment. Red curves: fitting curves based on Eq. (1) for different temperatures.

To clearly analyze the fitting results, we explicitly obtain the temperature-dependent fitting parameters  $A_{\text{fast}}$ ,  $A_{\text{slow}}$ ,  $A_{\text{slower}}$ ,  $\tau_{\text{fast}}$ ,  $\tau_{\text{slow}}$ , and  $\tau_{\text{slower}}$ , and summarize them in Fig. 4. In Figs. 4(a), 4(c), and 4(e) the amplitudes are displayed, and in Figs. 4(b), 4(d), and 4(f) the lifetimes are shown.

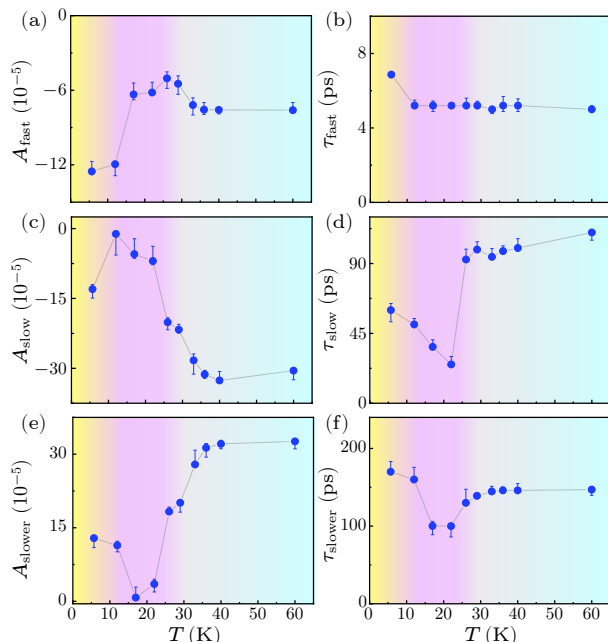


**Fig. 4.** Temperature dependence of the amplitudes (a)  $A_{\text{fast}}$ , (c)  $A_{\text{slow}}$ , (e)  $A_{\text{slower}}$  and lifetimes (b)  $\tau_{\text{fast}}$ , (d)  $\tau_{\text{slow}}$ , (f)  $\tau_{\text{slower}}$ , respectively. The yellow, purple, and pale blue zones together yield potential transitions at both  $T_c = 10$  K and  $T^* = 29$  K.

The  $A_{\text{fast}}$  initially increases with temperature at 10 K. Then it tends to decrease at 29 K, before reaching a constant value at higher temperatures ( $T > 36$  K) [Fig. 4(a)]. The  $A_{\text{slow}}$  curve exhibits a similar behavior as  $A_{\text{fast}}$  [Fig. 4(c)]. The  $A_{\text{slower}}$  initially decreases at 10 K and exhibits an increase at 29 K [Fig. 4(e)]. A commonly shared feature is that they both experience changes at around 10 and 29 K. For the lifetimes,  $\tau_{\text{fast}}$  exhibits a slight decrease from 7 ps at 5.7 K to 5 ps at 10 K [Fig. 4(b)], before resumes a constant value over the entire left region of temperature. Because there is only one datum point, this reducing value of  $\tau_{\text{fast}}$  may be a real change or an experimental data fluctuation, for which we leave to future investigations. The  $\tau_{\text{slow}}$  initially decreases with increasing temperature, even across 10 K, till at 22 K where it starts to increase. Around 29 K, it reaches its maximum and ceases increasing. It remains to be nearly a constant at about 100 ps for  $T > 29$  K [Fig. 4(d)]. The  $\tau_{\text{slower}}$  experiences a similar temperature dependence as  $A_{\text{slower}}$ . Its value decreases at 10 K and starts to increase in the 22–36 K range [Fig. 4(f)]. Indeed, for all the four parameters  $A_{\text{slow}}$ ,  $\tau_{\text{slow}}$ ,  $A_{\text{slower}}$ , and  $\tau_{\text{slower}}$ , one characteristic temperature is 10 K, which we define as  $T_c$ , and the other characteristic temperature is a range of 22–36 K, for which we define a characteristic average temperature  $T^* = 29$  K.

In Fig. 4, different colored backgrounds have been used to mark to potential phase transitions. The three ultrafast

relaxation components of  $\text{Ba}_6\text{Cr}_2\text{S}_{10}$  all exhibit changes in amplitudes and lifetimes at  $T_c = 10$  K and  $T^* = 30$  K. One phase transition occurs at  $T_c = 10$  K and the other might be a potential phase transition at  $T^* = 29$  K with a soft stiffness (22–36 K).<sup>[34]</sup> Such an observation is consistent with the direct time domain illustration shown in Fig. 2(c), which has a salient feature around 10 K and another milder color change at 22–36 K. The critical temperature  $T_c = 10$  K is consistent with the toroidal magnetic phase transition identified in Ref. [2]. Thus, we demonstrate that the TM-to-paramagnetic phase transition at around 10 K is observed by time-resolved ultrafast pump-probe dynamics. We assign the fast component to electron–phonon coupling and the slow component to phonon–phonon scattering. The slower component can be associated with various origins. It is unlikely to be due to the thermal effect, because the fluences are low. As there are rare related characterizations, we leave it to future investigations. The same applies to the A term.

The reason why a magnetic phase transition may affect the photocarrier dynamics might be understood as that there is a possible static coupling between the spin and lattice<sup>[29]</sup> and/or a spin-charge correlation that leads to a slight change in the lattice and electron density below  $T_c$ . Thus, the electron–phonon scattering and phonon–phonon scattering are modified. At above 10 K, the TM spin structure is replaced by a quasi-1D short-range spin ordering whereby the in-plane ferromagnetic ordering is greatly weakened. Our work thus motivates further identifications to resolve the complex structures in spin, lattice, and charge degrees of freedom, such as the temperature-dependent  $c$ -axis lattice constants in this quasi-1D system. Usually, from  $\tau_{\text{fast}}$  one can obtain the electron–phonon coupling strength. If the reduction in the value of  $\tau_{\text{fast}}$  is real [Fig. 4(b)], it exactly corresponds to the influence of such a static coupling between the spin and lattice at  $T_c = 10$  K. The ultrafast dynamics change we observed in all components might be an excited state evidence of the existence of the TM magnetic structure.

For the ultrafast dynamics variations in the temperature range 22–36 K, centered at  $T^* = 29$  K, we attribute them to another potential phase transition. As shown in the magnetic transport measurement (Fig. S4), our  $\text{Ba}_6\text{Cr}_2\text{S}_{10}$  sample displays a ferromagnetic phase transition near 30 K, which is in line with our ultrafast spectroscopy observation. It suggests that a less ferromagnetic impurity phase exists, although the powder X-ray diffraction shows almost a single phase of  $\text{Ba}_6\text{Cr}_2\text{S}_{10}$ . Note that the single crystal  $\text{Ba}_6\text{Cr}_2\text{S}_{10}$  we measure is picked out from polycrystalline samples synthesized under high temperature. Therefore, we attribute the potential phase transition observed in our experiment at 29 K to the unknown magnetic impurities on the surface of the sample. Note that the slow component mainly reflects the phonon–phonon scattering; spin-modified lattices will inevitably lead to modifications in such phonon–phonon scattering, too. Thus, the slow component of the ultrafast dynamics also manifests the influence of a possible static coupling between the spin and lattice. Consequently, all our ultrafast dynamics results also consistently demonstrate a potential



magnetic phase transition at  $T^* = 29$  K, too. Because we are in the linear regime, there is unlikely photoinduced electronic and structural transitions. Note that, for the possible static spin-lattice interaction mentioned above, it is still ultrafast dynamics modified by the magnetic phase transition.

In summary, we have investigated the ultrafast spectroscopy of a new magnetic material  $\text{Ba}_6\text{Cr}_2\text{S}_{10}$ . Using the modified ultrafast dynamics, we clearly observe the TM-paramagnetic phase transition at  $T_c = 10$  K. Moreover, we also demonstrate ultrafast dynamics evidence for the existence of an unknown magnetic phase transition at  $T^* = 29$  K. Our findings shed light on the further exploration of ultrafast dynamics and phase transitions in quasi-1D dimerized magnetic systems.

*Acknowledgement.* This work was supported by the National Key Research and Development Program of China (Grant Nos. 2021YFA1400201 and 2017YFA0303600), the CAS Project for Young Scientists in Basic Research (Grant No. YSBR-059), the Beijing Natural Science Foundation (Grant No. 4191003), the Strategic Priority Research Program of CAS (Grant No. XDB30000000), and the CAS Interdisciplinary Innovation Team.

## References

- [1] Fukuoka H, Miyaki Y, and Yamanaka S 2007 *Bull. Chem. Soc. Jpn.* **80** 2170
- [2] Zhang J, Wang X C, Zhou L, Liu G X, Adroja D T, da Silva I, Demmel F, Khalyavin D, Sannigrahi J, Nair H S, Duan L, Zhao J F, Deng Z, Yu R Z, Shen X, Yu R C, Zhao H, Zhao J M, Long Y W, Hu Z W, Lin H J, Chan T S, Chen C T, Wu W, and Jin C Q 2022 *Adv. Mater.* **34** 2106728
- [3] Fukuoka H, Miyaki Y, and Yamanaka S 2003 *J. Solid State Chem.* **176** 206
- [4] Wu Y L, Yin X, Hasaien J Z L, Tian Z Y, Ding Y, and Zhao J M 2021 *Rev. Sci. Instrum.* **92** 113002
- [5] Wu Y L, Yin X, Hasaien J, Ding Y, and Zhao J M 2020 *Chin. Phys. Lett.* **37** 047801
- [6] Tian Y C, Zhang W H, Li F S, Wu Y L, Wu Q, Sun F, Zhou G Y, Wang L L, Ma X C, Xue Q K, and Zhao J M 2016 *Phys. Rev. Lett.* **116** 107001
- [7] Giannetti C, Capone M, Fausti D, Fabrizio M, Parmigiani F, and Mihailovic D 2016 *Adv. Phys.* **65** 58
- [8] Crooker S A 2002 *Rev. Sci. Instrum.* **73** 3258
- [9] Rice W D, Liu W, Baker T A, Sinitsyn N A, Klimov V I, and Crooker S A 2016 *Nat. Nanotechnol.* **11** 137
- [10] Wang R, Wang T, Zhou Y, Wu Y L, Zhang X X, He X Y, Peng H L, Zhao J M, and Qiu X H 2019 *2D Mater.* **6** 035034
- [11] Toda Y, Kawanokami F, Kurosawa T, Oda M, Madan I, Mertelj T, Kabanov V V, and Mihailovic D 2014 *Phys. Rev. B* **90** 094513
- [12] Kabanov V V, Demsar J, Podobnik B, and Mihailovic D 1999 *Phys. Rev. B* **59** 1497
- [13] Cao N, Wei Y F, Zhao J M, Zhao S P, Yang Q S, Zhang Z G, and Fu P M 2008 *Chin. Phys. Lett.* **25** 2257
- [14] Cao N, Long Y B, Zhang Z G, Yuan J, Gao L J, Zhao B R, Zhao S P, Yang Q S, Zhao J M, and Fu P M 2008 *Physica C* **468** 894
- [15] Wu Q, Zhou H X, Wu Y L, Hu L L, Ni S L, Tian Y C, Sun F, Zhou F, Dong X L, Zhao Z X, and Zhao J M 2020 *Chin. Phys. Lett.* **37** 097802
- [16] Luo C W, Wu I H, Cheng P C, Lin J Y, Wu K H, Uen T M, Juang J Y, Kobayashi T, Chareev D A, Volkova O S, and Vasiliev A N 2012 *Phys. Rev. Lett.* **108** 257006
- [17] Chia E E M, Talbayev D, Zhu J X, Yuan H Q, Park T, Thompson J D, Panagopoulos C, Chen G F, Luo J L, Wang N L, and Taylor A J 2010 *Phys. Rev. Lett.* **104** 027003
- [18] Wang M C, Qiao S, Jiang Z, Luo S N, and Qi J 2016 *Phys. Rev. Lett.* **116** 036601
- [19] Sun F, Zhang T, Yi C J, Wu Y L, Zhao H, Wu Q, Shi Y G, Weng H M, and Zhao J M 2021 *Phys. Rev. B* **104** L100301
- [20] Sun F, Wu Q, Wu Y L, Zhao H, Yi C J, Tian Y C, Liu H W, Shi Y G, Ding H, Dai X, Richard P, and Zhao J M 2017 *Phys. Rev. B* **95** 235108
- [21] Wu Q, Sun F, Zhang Q Y, Zhao L X, Chen G F, and Zhao J M 2020 *Phys. Rev. Mater.* **4** 064201
- [22] Yu B H, Tian Z Y, Sun F, Peets D C, Bai X D, Feng D L, and Zhao J M 2020 *Opt. Express* **28** 15855
- [23] Zhao J M, Bragas A V, Lockwood D J, and Merlin R 2004 *Phys. Rev. Lett.* **93** 107203
- [24] Zhao J M, Bragas A V, Merlin R, and Lockwood D J 2006 *Phys. Rev. B* **73** 184434
- [25] Huang Y X, Zhao H, Li Z L, Hu L L, Wu Y L, Sun F, Meng S, and Zhao J M 2023 *Adv. Mater.* **35** 2208362
- [26] Ji B Y, Jin Z M, Wu G J, Li J G, Wan C H, Han X F, Zhang Z Z, Ma G H, Peng Y, and Zhu Y M 2023 *Appl. Phys. Lett.* **122** 111104
- [27] Hasaien J, Wu Y L, Shi M Z, Zhai Y N, Wu Q, Liu Z, Zhou Y, Chen X H, and Zhao J M 2023 submitted
- [28] Han X F, Weng Y X, Wang R, Chen X H, Luo K H, Wu L A, and Zhao J M 2008 *Appl. Phys. Lett.* **92** 151109
- [29] Hu L L, Yang M, Wu Y L, Wu Q, Zhao H, Sun F, Wang W, He R, He S L, Zhang H, Huang R J, Li L F, Shi Y G, and Zhao J M 2019 *Phys. Rev. B* **99** 094307
- [30] Morandi O, Hervieux P A, and Manfredi G 2009 *Eur. Phys. J. D* **52** 155
- [31] Smith D C, Gay P, Stevens C J, Chen C, Yang G, Abell S J, Wang D Z, Wang J H, Ren Z F, and Ryan J F 2000 *Physica C* **341** 2221
- [32] Matsuda T, Nishibayashi K, and Munekata H 2014 *Proc. SPIE* **9167** Spintronics VII 91670M
- [33] Tian Z Y, Zhang Q Y, Xiao Y W, Gamage G A, Tian F, Yue S, Hadjiev V G, Bao J M, Ren Z F, Liang E J, and Zhao J M 2022 *Phys. Rev. B* **105** 174306
- [34] Wang R, Zhou J B, Wang X S, Xie L M, Zhao J M, and Qiu X H 2021 *Nano Res.* **14** 1162